LA-UR -81-805

CONF-810314--103

TITLE: BEAM CHARACTERISTICS IN THE LAMPF BIOMEDICAL CHANNEL

MASTER

AUTHOR(S): M. Paciotti, J. Bradbury, H. Inoue, O. Rivera, and S. Sandford

SUBMITTED TO: IEEE 1981 Particle Accelerator Conference, Washington, DC, March 11-13, 1981

University of California

LOS ALAMOS SCIENTIFIC LABORATORY
Post Office Box 1663 Los Alamos, New Mexico 87545
An Affirmative Action/Equal Opportunity Employer

Form No. 836 R3
St. No. 2629
12/78

UNITED STATES
DEPARTMENT OF ENERGY
CONTRACT W-7405-ENG. 36

BEAM CHARACTERISTICS IN THE LAMPF BIOMEDICAL CHANNEL*

M. Paciotti, J. Bradbury, H. Inoue, O. Rivera and S. Sandford
Los Alamos National Laboratory
Los Alamos, New Mexico 87545

Summary

We report on techniques to determine the muon component in the pion therapy beams at the Clinton P. Anderson Meson Physics Facility biomedical channel. The objective is to provide input to the project's treatment planning code PIPLAN which uses measured beam data to generate dose distributions. In these data it is important to identify the particles emanating from the channel by type, i.e., pion, muon, or electron. Muons from decays in the latter portion of the channel form a large "halo" around the pion beam. As our pion field sizes have increased, this "halo" has become an increasingly larger fraction of the beam. Results from beam measurements and computer simulations are presented.

Channel and Measuring Equipment

The channel has 11 magnetic elements in a three-bend system (Fig. 1)[1]. The first section collects pions and acts as a broad-band spectrometer. It focuses a dispersed beam with large momentum spread on a Be wedge degrader which reduces the spread to 1.6 percent rms $\Delta p/p$. Following the degrader a 60^0 wedge focusing bend directs the beam vertically downward into the beam-shaping section of five 35-cm bore quadrupole magnets. Multiwire proportional chambers are located before the last bend and above the beam-shaping section. The last bend serves as a magnetic spectrometer, allowing momentum measurement of each particle. Chamber planes at the channel exit complete the system comprising a total of 10 planes in coincidence along with time-of-flight scintillators.

The important feature is that the particle trajectory is determined above and below the quadrupole section. Data is collected at reduced primary beam current to permit proper chamber performance.

Time-of-Flight Measurements

Figure 2 shows the time-of-flight distribution through the 11.7 m channel using a chopped proton beam for which the micropulse separation is 40 ns instead of the usual 5 ns. The accelerator radio frequency signal provides the timing reference. The width of the electron peak indicates that the overall resolution is about 0.5 ns rms which contains contributions from the micropulse length on target, resolution of the electronics, scintillator size effects, and path length differences through the channel. A 10% reduction in width is observed when the channel acceptance is stopped down and is consistent with calculated path length differences.

The intrinsic 0.5 ns width of the pion peak is further increased by the large momentum spread of the beam in the 4.7 m before the degrader. The momentum of each particle before entering the wedge is measured by its focal plane position,[1] limited in accuracy by wedge scattering. The momentum of each particle is directly measured after the wedge using the last bend, and therefore an accurate time correction is possible for the 7 m region to the end of the channel. After both corrections, the time width of the pions alone can be reduced to the electron width.

Prior to the availability of chopped beams, time-of-flight was measured between two scintillators, one 4.3 m upstream in the channel and one at the exit. In addition, the 201 MHz reference signal was used to get total flight time in the channel as indicated earlier. This spectrum alone cannot resolve pions and muons since it is not known which micropulse initiated the event. This ambiguity is approximately resolved by taking into account the flight time between the two scintillators. Figure 3 is the pion-muon region so obtained. The chopped beam data is preferred, and is used for following results.

Results of Time-Of-Flight Data

Electron contamination has been discussed previously.[2] Pion decays in the target region produce so-called "cloud" muons which are also seen as a peak in Fig. 2. Decays along the channel fill the valley between the cloud muon and pion peaks. Within the pion peak are muons from decays in the latter part of the channel.

After momentum correction, the pion peak is Gaussian-fitted, and a cut is made at 2.5 σ toward the muon region separating out pions and muons from late decays from the identifiable muons. The fractions of the total beam for each component are given in Table I for three momenta. The pion-muon division is dependent on resolution for a particular run so these numbers are not exactly the same for every run of the same momentum.

Detection of Decays in Latter Part of Channel

As particle trajectories are measured before and after the beam section where decays are not identified by time, it is easy in principle to identify late decays. The matrix transformation from the upper wire chambers to the lower wire chamber predicts the output trajectory from the measured trajectory at the upper chambers. We form these differences for each event:

$$\Delta_X = X_{measured} - X_{predicted}$$

$$\Delta_\theta = \theta_{measured} - \theta_{predicted}$$

$$\Delta_Y = Y_{measured} - Y_{predicted}$$

$$\Delta_\phi = \phi_{measured} - \phi_{predicted}$$

The distributions of the Δ's are Gaussian with long tails that are identified as muons from decays in the region between the chambers. The widths of the pion central regions are typically 1-2 cm rms and 10-20 mr rms. Multiple scattering due to material in the beam such as the wire chambers themselves contribute to the widths. The channel has no vacuum system and has He bags most of the length of the channel.

Figure 4 is a scatterplot of Δ_θ vs. time-of-flight. The pion region shows long tails due to decays in the 4 m between the upper and lower chambers; the tails are much smaller in the cloud muon and electron regions. The tails are thus seen as evidence for kinks in the trajectories and are

*Work supported by US PHS grant CA-16127 from NCI, and US Department of Energy.

identified as muons. A similar scatterplot can be made for a pion beam with a small spot size if X is plotted directly against time. The usual muon halo is then evident. Using the Δ's just makes this halo visible for wide beams. The muons identified by kinks have the same momentum distribution as their predecessor pions for which the momentum was measured through the last bend.

Computer Simulation

The muon decay problem has been simulated with the ray-tracing code DECAY TURTLE[3] which was modified for this particular problem. Quantities exactly equivalent to the Δ's were calculated including appropriate multiple-scattering in the channel provided by TURTLE in the usual way. The Δ's observed in the channel are fitted by a Gaussian-weighted moment calculation. The muon tails are effectively ignored. The widths of these fits are largely explained by the multiple-scattering in the TURTLE calculations.

Another question answered by TURTLE refers to the muons unseen within the pion time-of-flight peak, i.e., those particles within 2.5 σ of the pion peak. Specifically, how many of these muons originate prior to the upper wire chambers? In these instances the kink method is not applicable. Depending on momentum, only 3-5% of the muons inseparable by time, originate between the wedge degrader and the upper wire chambers.

With decays turned on, the Δ's calculated in TURTLE contain the long tails from the muon events. The same Gaussian-weighted fitting is done to obtain the widths of each Δ. Events outside ±2.5 σ on any of the four Δ's are flagged as muons. The widths of the experimental Δ's can also be used without substantial change in the result. How many muons would be missed by this procedure? Extreme backward or forward decays fall into this class. The result is that 3-5% of the muons detected in the wire chambers but not separable from pions by time-of-flight will not exhibit sufficient kinks to be flagged as muons.

Results of TURTLE Calculations

Table II gives the TURTLE results for muons that hit the 40 x 40 cm time-of-flight counter but are not separable from pions by time-of-flight. Column 5 gives the μ/π ratio for those particles for several types of tunes. This information completes the picture of beam composition. For example, the 71% π + μ at 150 MeV/c in Table I becomes 60% π and 11% μ using μ/π = 0.18.

In addition, a large number of muons miss the time-of-flight counter entirely. In the 150 MeV/c example, this component is equal to the number given in column 5, leaving the total composition barely over 50% pions in this case. These extremely wide muons should be stopped prior to the patient but are not otherwise any problem.

Fractional composition alone is not useful for most purposes. The phase space of each muon component is very different. The muons in Table I have roughly the phase space of the pion beam. The muon distributions due to decays late in the channel given in column 5 are broad with large angles. Column 6 gives the μ/π ratio at the center of the field for these muons and reflects the relative sizes of pion and muon distributions.

The last two tune types show reduced muon fraction in the center of the field. The patient is scanned beneath such beams in the dynamic treatment mode.[2] With proper collimation, a large fraction of the muon halo can be eliminated.

Experimental Situation on Kink Detection

The experimental situation for kink detection is not as clean as the TURTLE result. The problem is that a significant number of pions can be incorrectly flagged as muons. That is, significant numbers of pions fall outside the ±2.5 σ cuts on the Δ's. Direct tests can be made for e^- and cloud μ^- where kinks are not expected. At 150 MeV/c only about 3% of the e and cloud μ would be flagged as having a kink using the same procedure. However, at the higher momenta, the fraction is up to 4% for e^- and 10% for cloud μ^-.

The situation is improved by making the cuts on the Δ's at ±3 σ. Twice as many muons will be missed but fewer pions will be misidentified as muons. With ±3 σ the particles flagged as late decays are approximately the same as predicted by TURTLE in number and phase space distribution.

Conclusion

We have identified contamination fractions in our beams but are not yet satisfied with correct identification of muons within the pion time-of-flight peak. Forward decays are the most difficult to handle, and an additional signature for them such as range discrimination is needed. However, the added drift for such a measurement introduces more muons.

The methods described here are probably sufficient to experimentally reject the late decay component rather than to identify a pure sample. The late decays would be then entirely calculated for PIPLAN input, with the added advantage of giving properly correlated momenta and polarizations.

References

1. Paciotti, M.A., Bradbury, J.N., Holland, J.A., Hutson, R.L., Knapp, E.A., Rivera, O.M., Knowles, H.B., and Pfeuffer,G.: Tuning of the first section of the biomedical channel at LAMPF. IEEE Trans. Nucl. Sci. 22: 1784, 1975.

2. Paciotti, M., Amols, H., Bradbury, J., Rivera, O., Hogstrom, K., Smith, A., Inoue, H., Laubacher, D., and Sandford, S.: Pion beam development for the LAMPF biomedical project. IEEE Trans. Nucl. Sci. NS-26 3071-3073, 1979.

3. Brown, K.L. and Iselin, Ch. : DECAY TURTLE (Trace Unlimited Rays Through Lumped Elements), A computer program for simulating charged particle beam transport systems, including decay calculations. CERN 74-2, 5 February 1974.

TABLE I

Beam Composition from Time-of-Flight Data.
Muons from late decays are not separated from pions.

Momentum (MeV/c)	π^- and μ^- From Late Decays	Cloud μ^- and μ^- From Mid-Channel Decays	e^-
150	71%	15%	14%
167	75%	16%	9%
190	81%	12%	7%

TABLE II

TURTLE Results for Muons Within the Pion Time-Of-Flight Peak and Hitting 40 x 40 Cm Scintillator

Beam Type-Treatment Mode[7]	Pion Beam Size FWHM(cm) X	Y	Momentum MeV/c	$\frac{\mu}{\pi}$	μ/π On Axis
Broad-Static	16	15	150	0.18	0.051
Broad-Static	17	20	150	0.18	0.074
Broad-Static	16	15	167	0.19	0.060
Broad-Static	20	23	167	0.18	0.092
Broad-Static	18	16	190	0.20	0.094
Broad-Static	22	22	190	0.20	0.14
Fan-Dynamic	23	3	167	0.18	0.025
Spot-Dynamic	5	7	167	0.21	0.018

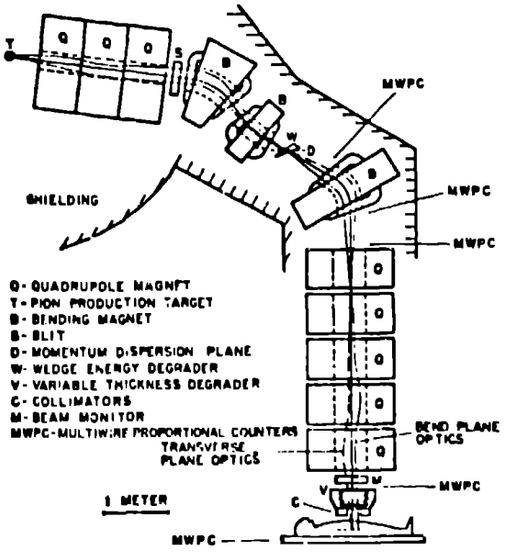

Fig. 1 Channel layout showing locations of multiwire proportional chambers.

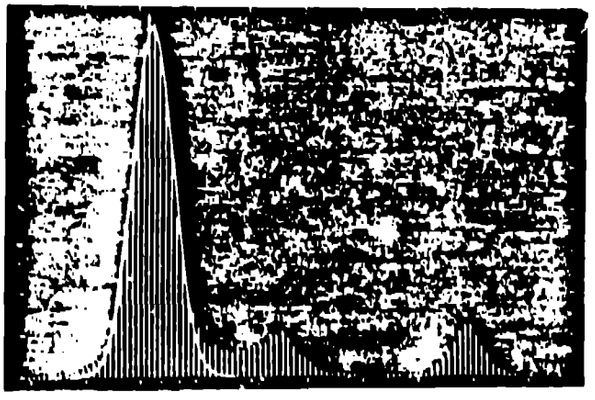

Fig. 2 Time-of-flight distribution for 167 MeV/c negative beam using 40 ns chopped proton beam. Width of pion region fit is 0.75 ns.

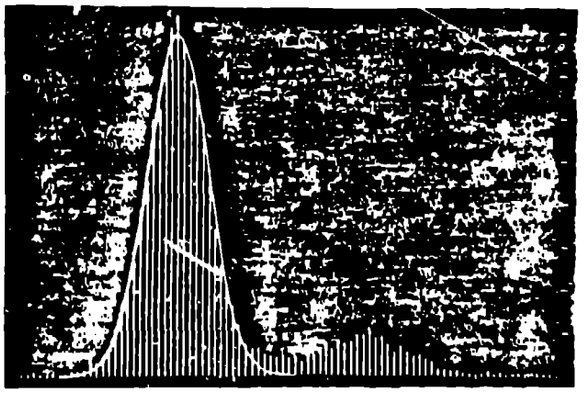

Fig. 3 Time-of-flight distribution 167 MeV/c beam. Shows π-μ region only. Uses unchopped proton beam and time-of-flight through 11.7 m channel. Also uses time between two scintillators with 4.3 m separation to resolve ambiguity due to 5 ns spaced micropulses. Width of pion region fit is 0.75 ns rms.

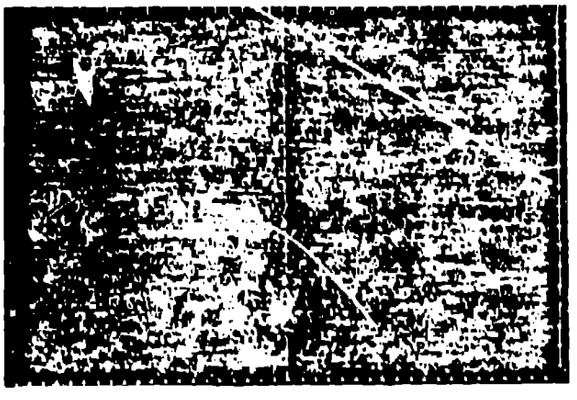

Fig. 4 Scatter plot of events in a rge therapy beam. Horizontal axis is Δ_θ, deviation of output angle θ from expected angle based on its trajectory earlier in channel. Vertical axis is time-of-flight showing π^--μ^--e^- regions. Pion decays in last 4 m of channel show up as the long tails extending out from the pion region.